



Experimental and numerical investigations on push-out delamination in drilling of composite laminates

R. Higuchi^{a,*}, S. Warabi^b, W. Ishibashi^b, T. Okabe^{b,c}

^a Department of Aeronautics and Astronautics, The University of Tokyo, 7-3-1 Hongo, Bunkyo-ku, Tokyo, 113-8656, Japan

^b Department of Aerospace Engineering, Tohoku University, 6-6-01, Aramaki-Aza-Aoba, Aoba-ku, Sendai, Miyagi, 980-8579, Japan

^c Department of Materials Science and Engineering, University of Washington, 302 Roberts Hall, Seattle, WA, 98195, USA

ARTICLE INFO

Keywords:

Drilling
Delamination
Damage mechanics
Finite element analysis (FEA)
Non-destructive testing

ABSTRACT

This study conducts experimental and numerical studies on the progressive damage occurring during the drilling of composite laminates. In particular, this work focuses on push-out delamination, which occurs at the interface around the drill-exit and is the most critical damage suffered during the drilling process. To investigate the damage progression mechanisms, penetration and interruption drilling tests are performed on composite laminate consisting of quasi-isotropic CFRP plies and fabric GFRP ply (bottom side). After drilling tests, the damage evolution is evaluated using X-ray computed tomography and optical microscopy. Based on the experimental results, a simplified simulation model is established, and damage progression simulation is performed using an explicit dynamic finite element method. The results show that the bending deformation in the bottom two plies triggers the propagation of push-out delamination. Therefore, the extent of delamination is significantly affected by the thickness and the material properties of the bottom plies.

1. Introduction

Drilling of composite laminates and the associated internal damages are critical issues in aircraft manufacturing. Although drilling is an essential process during the assembly of several parts, the thrust force from the drill tip and the peeling up from the drill edge often trigger various kinds of internal damage (e.g., fiber pull-out, matrix crack, and peel-up/push-out delamination) around the hole. Most of these damages occurred within the diameter of the drill and are removed by the drilling process. However, inappropriate drilling conditions can cause significant damage, and the damage left around the hole can negatively affect the quality of the hole [1–3].

Over the past few decades, several experimental studies have been conducted to investigate the internal damage during the drilling process [4–14]. These studies have revealed that push-out delamination is the most critical type of internal damage [5–8]. Liu et al. [4] reported that this delamination is induced by a combination of the thrust force and the reduction of the bending stiffness of the un-processed part due to a decrease in thickness by drilling. Therefore, the initiation and propagation of this delamination during the drilling process depends not only on drilling conditions (feed rate [6–13], spindle speed [6–12], drill shape [10–13], drill wear [14], etc.), but also on the material property

[9,15], stacking sequence [9], ply thickness, and other such parameters. These findings have been obtained empirically based on many parametric studies with different drilling conditions and are not based on the theoretical background. Although many experimental studies have investigated delamination, all of these studies have only evaluated the delamination in completely drilled specimens; the detailed initiation and propagation mechanism of push-out delamination during the drilling process has not been completely clarified yet. To the best of the authors' knowledge, no previous work has investigated the damage evolution during the drilling process. The authors believe that it is impossible to determine the drilling condition theoretically (not empirically) without a comprehensive understanding of the mechanism of push-out delamination. In fact, practical drilling conditions in aircraft manufacturing are primarily determined based on empirically derived criteria or by trial and error.

Numerical studies [2,9,16–18] that use the finite element method (FEM) have recently increased as a result of improvements in computational power and the development of simulation techniques. Models used in previous numerical studies can be separated into two categories; (i) complete simulation models [16–18] and (ii) simplified simulation models [2,9,18]. Complete simulation models consider almost all phenomena in the drilling process. In these models, a drill model with an

* Corresponding author.

E-mail address: higuchi@aastr.t.u-tokyo.ac.jp (R. Higuchi).

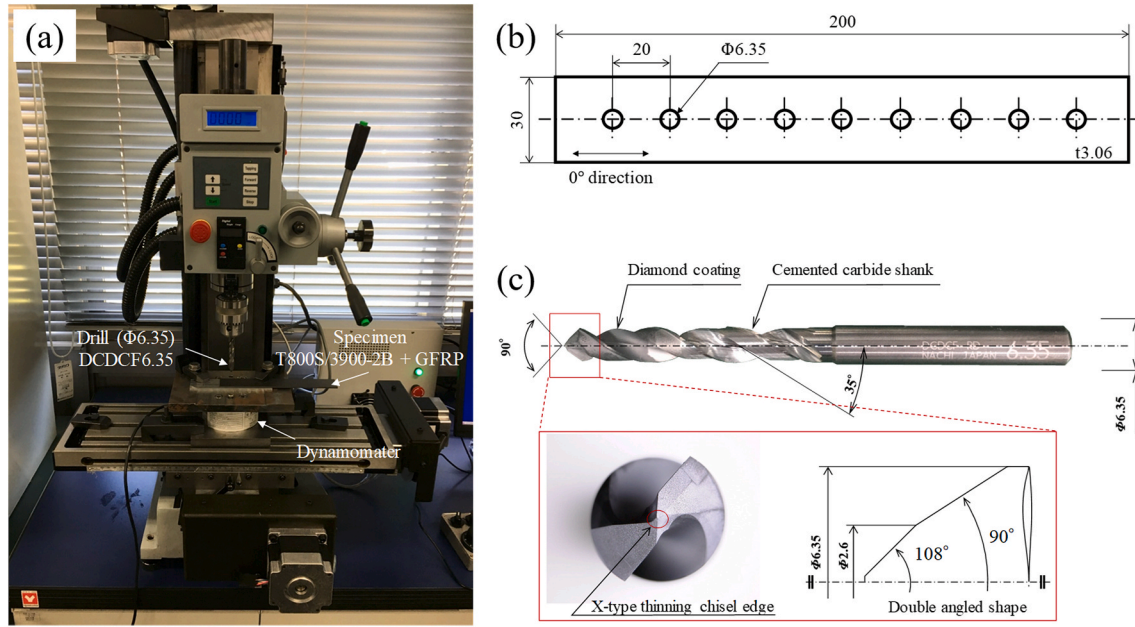


Fig. 1. Schematic diagram for the drilling experiment system.

accurate shape is introduced, and both feed rate and spindle rate are imposed on it. In contrast, simplified simulation models neglect the effect of torque and simplify the drilling process into a quasi-static bending problem. This is because it has been reported that the thrust force has a greater effect on the push-out delamination than torque [4]. This simplification enables us to avoid performing a dynamic simulation with high computational cost due to the numerous eroding elements [18]. However, it is difficult to predict the delamination area quantitatively under various drilling conditions, even when a complete simulation model is used. To improve the prediction accuracy, we believe that the damage modelling strategy should be verified by detailed comparisons with experimental results in terms of both the final damage left around the completely drilled holes and the intermediate damage during the drilling process.

Therefore, the aims of this study are (i) to clarify the damage initiation and propagation mechanisms using experiments, and (ii) to develop and verify an experiment-based mesoscale damage model for drilling simulation. First, penetration and interruption drilling tests and two kinds of damage observations on the specimens are conducted to investigate the damage mechanisms during drilling. The experimental setup, procedures, and results are summarized in Section 2. Second, we develop a simplified simulation scheme with mesoscale damage models that is based on experimental observations. The details of the damage modelling strategy, verification against the experimental results, and some sensitivity studies are described in Section 3. Finally, we present the conclusions of the present work in Section 4.

2. Experiments

In this study, two kinds of experiments were conducted; penetration and interruption tests. In the former, complete holes were drilled at different feed rates to examine their effects on the push-out damage behavior. In the latter, the drilling process was interrupted at several characteristic points on the thrust force-displacement response. For a detailed investigation of internal damage progression, all manufactured holes were investigated using X-ray Computed Tomography (CT) and cross-section observations by optical microscopy. The details of the test procedure are summarized below.

2.1. Testing procedure

The experimental setup is depicted in Fig. 1 (a). The experimental setup and conditions were determined on the basis of previous studies [13,14]. All drilling experiments were conducted using an NC milling machine (PSF550-CNC, Prospec Industry Co., Ltd.) with a maximum spindle speed of 3200 rpm. The thrust force and torque were measured using a 6-axis force sensor (PFS100YS302U6, Leptrino Co. Ltd.) that was placed behind the specimen. The specimens were prepared using T800S/3900-2B (Toray) unidirectional tape. The basic stacking sequence was as follows: 16 plies of quasi-isotropic laminates $[0/-45/90/45]_{2S}$ were stacked, and a woven GFRP ply $[0,90]$ was placed at the bottom. The addition of this ply at the bottom is standard procedure in the aircraft industry to prevent push-out delamination. The specimen dimensions were 200 mm (length) \times 30.0 mm (width) \times 3.06 mm (thickness) (CFRP: 3.00 mm and GFRP: 0.06 mm). In all, nine holes were drilled per specimen at intervals of 20.0 mm along the fiber direction of 0° ply. Specimen geometries are shown in Fig. 1 (b). The specimen was clamped with two knock pins on a backup plate with a hole. The diameter of the hole was large enough (20.0 mm) to mitigate the effect of the backup plate [18]. In fact, drilling in the aircraft industry is conducted without any backup plate. A crystal diamond coated twist drill with a diameter of 6.35 mm (DCDCF03650, Nachi-Fujikoshi Corp.) was used in this study. The shape and dimensions of the drill are illustrated in Fig. 1 (c).

Two kinds of observations were made on all drilled holes for damage characterization. First, three-dimensional damage distribution was observed using X-ray computed tomography (ScanXmate-D225RSS270, Comscantecno Co., Ltd.). The X-ray voltage was 70 kV, and the current was 90 μ A. Moreover, cross-sectional observation was performed using an optical microscopy (VHX-900, Keyence Corp.). The workpiece was cut parallel to 0° plies using a fine cutter and embedded in epoxy. Then, the surface of the cross-section was polished by buffing with diamond abrasive grains ($\varphi = 1, 3 \mu\text{m}$).

2.2. Penetration test and results

Penetration tests were carried out at a constant spindle speed (3200 rpm) and different feed rates (120, 375, 500, and 750 mm/min) to investigate the effect of feed rate on the thrust history and damage left

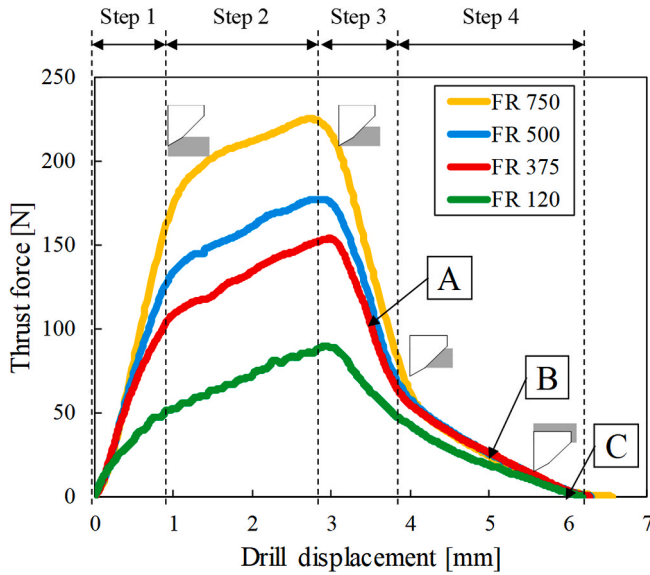


Fig. 2. Thrust force-displacement curves with feed rates of 120, 375, 500, and 750 mm/min.

around the completed holes. The drilling conditions were determined based on the factory-recommended values (spindle speed of 3200 rpm and feed rate of 375 mm/min) to explore drilling behaviour under realistic manufacturing conditions. To ensure repeatability, two specimens were tested at each feed rate. Fig. 2 shows the relationships between the thrust force and drill tip displacement. At all feed rates, the thrust force reached its maximum around 3 mm displacement, i.e., where the drill tip penetrated the lowermost layer. Thrust history can be divided into four stages. During Stages 1 and 2, thrust force linearly increases with the high and low gradients, respectively. Then, it decreases with the high and the low gradients during Stages 3 and 4. This change in thrust history corresponds to the change in the point angle of the drill. As shown in Fig. 1 (c), the point angle of the drill is not constant from the center to the edge. The point angles are 180° at the chisel edge region from the center to 0.1 mm radius, 108° from 0.1 mm to 1.3 mm

radius, and 90° from 1.3 mm to 3.175 mm radius. This means that the more central region of the drill can impart a higher reaction force in the feeding direction per unit radius. Therefore, the gradient of thrust history increases when the central region contacts the specimen or penetrates the specimen. Consequently, it can be concluded that the trend of thrust history is independent of the feed rate, but dependent on the contact condition between the drill and the specimen. This contact condition can be characterized by the specimen thickness, the drill geometry, and the drill position.

Fig. 3 summarizes the back views of the specimen and the X-ray CT images of the 16-ply of CFRP at different feed rates. Push-put delamination occurs at all feed rates (even at rates below the recommended value of 375 mm/min). The delamination mainly propagates in the fiber direction of the outermost CFRP layer, but its shape is asymmetrical owing to the effect of drill rotation. Basically, delamination increases with feed rate. In particular, at a feed rate of 750 mm/min, the outermost plies exhibited considerable push-out and showed significant delamination. As a result, the quality of the drilled hole shape was very poor. It is worth noting that very few little damage occurred in the plies, except for the drill entry and exit, even at the highest feed rate, as shown in Fig. 4. Fig. 4 indicates that the push-out delamination at the drill exit is much more significant than the peel-up delamination at the drill entry, which agrees with results obtained in previous studies [5–8]. Thus, we only focus on the push-out delamination in this work; the peel-up delamination is not included within the scope of this paper.

The cross-section image along with the 0° direction at the hole periphery at a feed rate of 750 mm/min is shown in Fig. 5. It is worth noting that the push-out delamination does not progress at the ply interface, but inside the CFRP 16-ply. Strictly speaking, this type of composite fracture is called "splaying", not delamination. However, the authors believe that the mechanism of splaying in this study is the same as that of the push-out delamination reported in previous studies—both fractures are mainly caused by the thrust force. The difference in fracture location is thought to be caused by the difference between the critical energy release rate at the ply interface of the material used in this study and the materials used in previous studies. In conventional CFRP laminates, the resin-rich region around the ply interface is the weakest location and easily suffers delamination under out-of-plane deformation. However, the material used in this study (T800S/3900-2B)

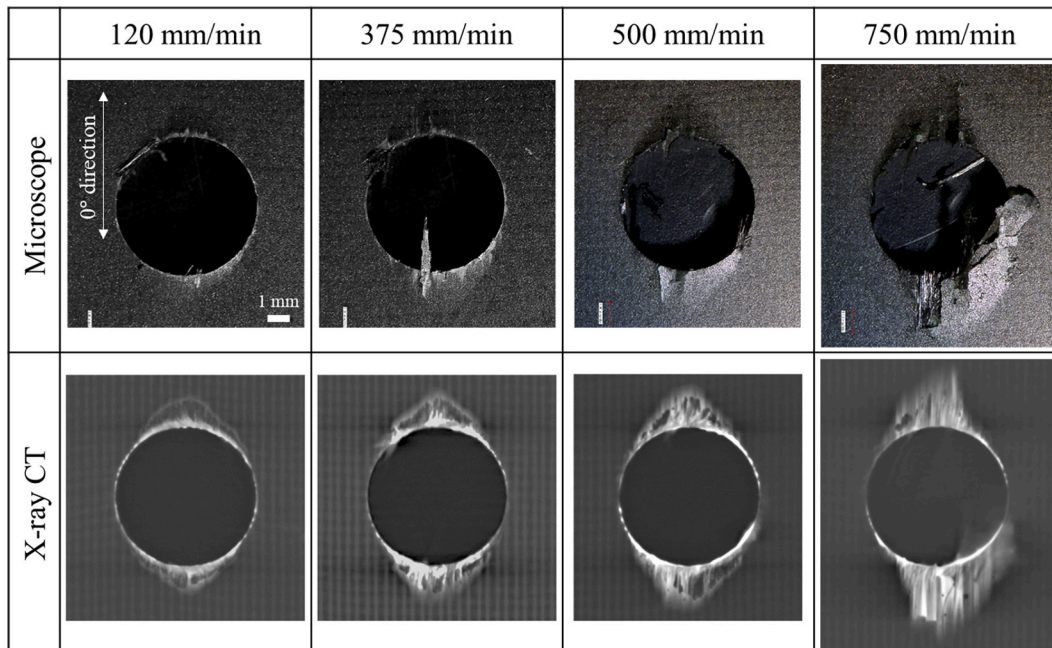


Fig. 3. Damage behaviors at the hole periphery with feed rates of 120, 375, 500, and 750 mm/min.

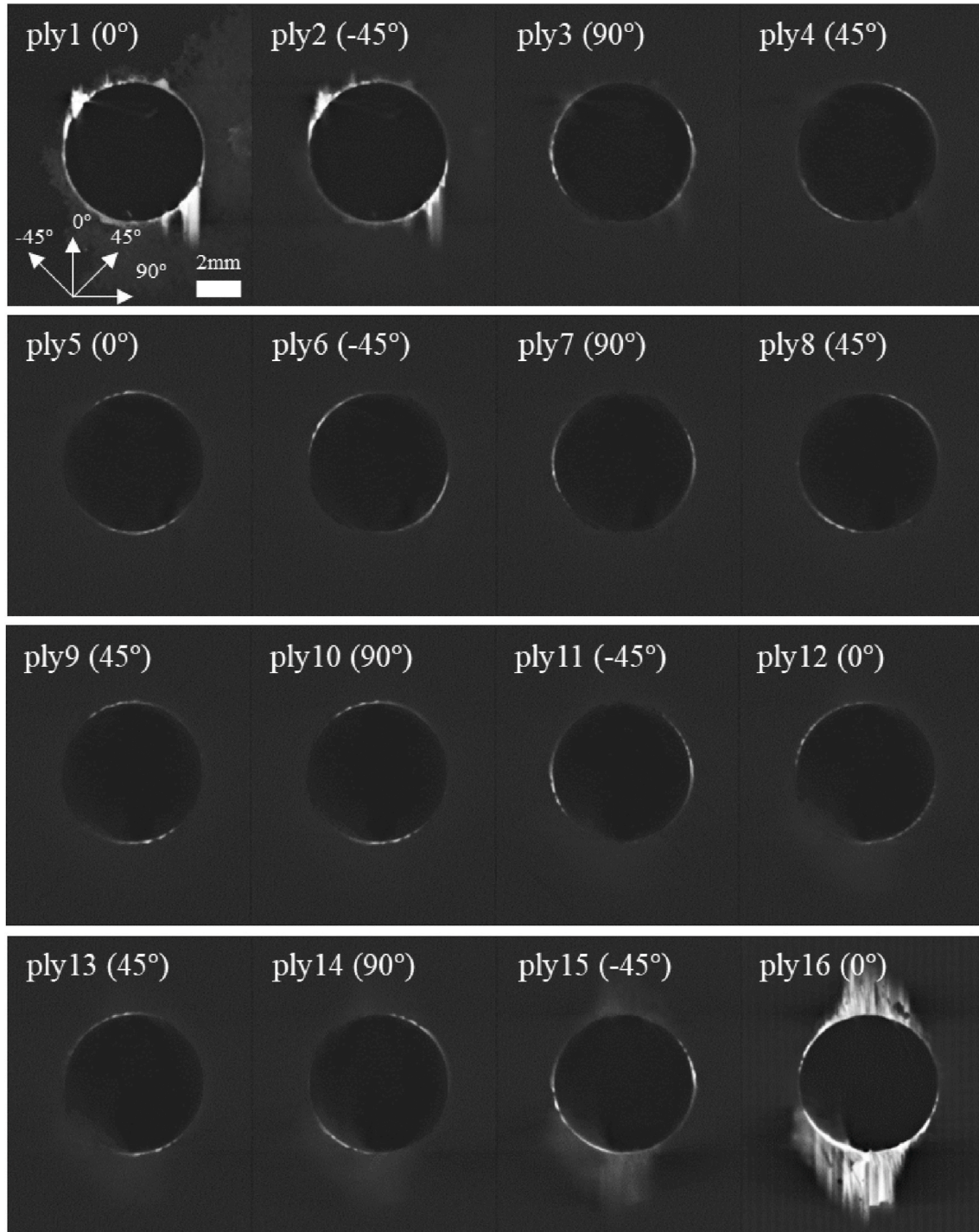


Fig. 4. Through-thickness damage distribution at a feed rate of 750 mm/min.

contains particles made of a thermoplastic resin at the ply interface to enhance the fracture toughness. The critical energy release rate at the ply interface is larger than that inside the ply. As a result, the fracture location is changed from the ply interface to the interior of the ply. Therefore, it was inferred that the push-out fracture occurs at the weakest location around the drill exit, and that there is no difference between the mechanisms of splaying and delamination. To maintain consistency in terminology with previous studies, splaying is referred to as “push-out delamination” in this work, although it occurs in the interior of the specimen.

2.3. Interruption tests and results

The interrupted drilling tests were conducted at a spindle speed of 3200 rpm and a feed rate of 375 mm/min. In this test, the feed was stopped at drill tip displacements of 3.9, 5.0, and 6.0 mm which were named points A, B, and C, respectively (as illustrated in Fig. 2). The drill was pulled out from the workpiece immediately after the feed was stopped. The interrupted displacement was set at characteristic points in the thrust force history obtained from penetration tests with the same drilling conditions shown in Fig. 2. This is because the characteristic point in the thrust force history is considered as the point where the

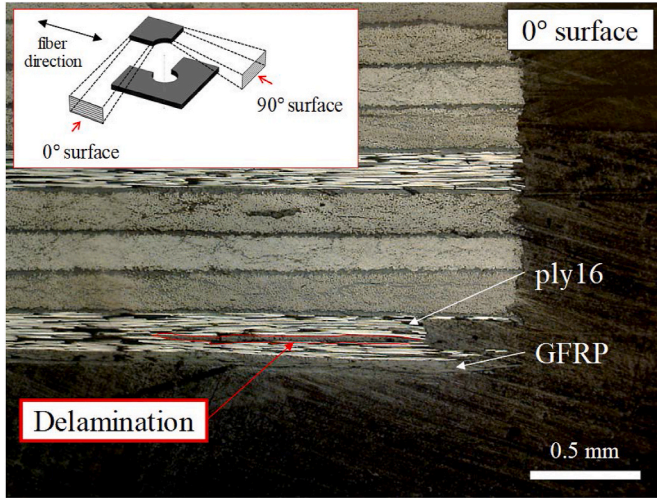


Fig. 5. Cross-section image along with the 0-degree direction at a feed rate of 750 mm/min.

stiffness reduces by internal damages or where the contact condition between the drill and laminate changes.

Fig. 6 shows the back and front views of the specimen and X-ray CT images of the CFRP 16-ply at each interrupted displacement. At point A, immediately after the drill penetrated the final layer, a cross-shaped crack was formed. This consisted of the transverse crack and fiber breakage in the CFRP 16-ply and fiber breakage in the GFRP ply. This crack propagated along the fiber direction of the CFRP 16-ply rather than the transverse direction. This is because less energy is required to form transverse cracks than to form fiber breakages in the CFRP 16-ply. Furthermore, the formation of this cross-shaped crack was accompanied by push-out delamination. At point B, although the drill tip was located 1.1 mm away from the penetration point, only a small portion of the two outermost plies were removed. Most regions were not drilled but bent by the thrust-force since the cross-shaped crack made around point A reduced the bending stiffness of the unprocessed region. At this point, several transverse cracks formed in the CFRP 16-ply and divided the remaining region into several strips. This lowered the bending stiffness of the unprocessed region. Until point C, the push-out delamination was continuously propagated by the out-of-plane bending of the unprocessed region. At this point, the delamination reached almost the same size as the final delamination. Therefore, it was assumed that the drilling

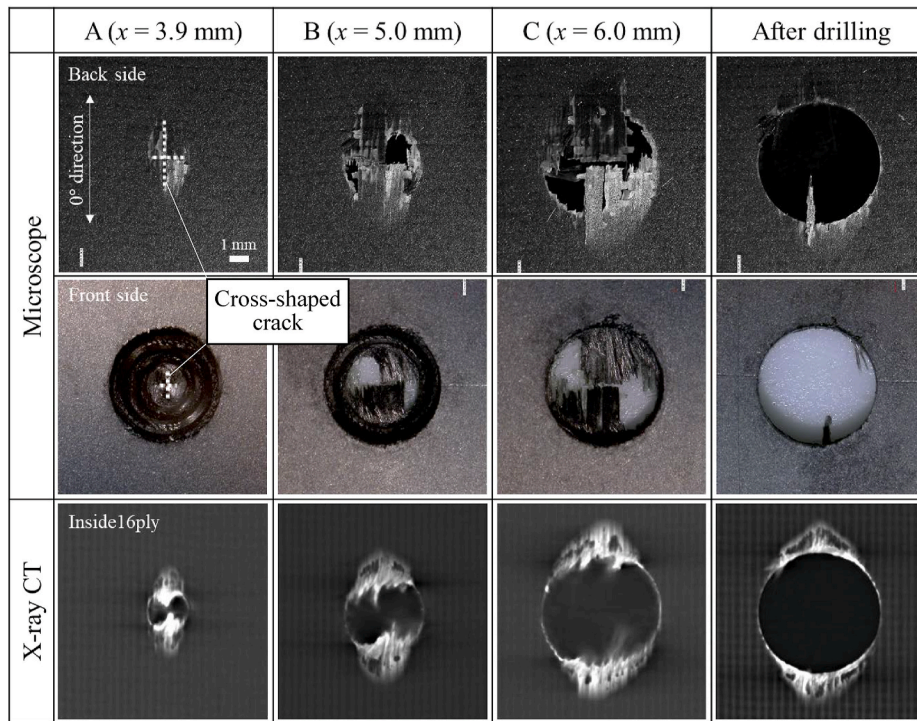


Fig. 6. Damage process observations at each drill tip displacement obtained in the interruption test with a feed rate of 375 mm/min.

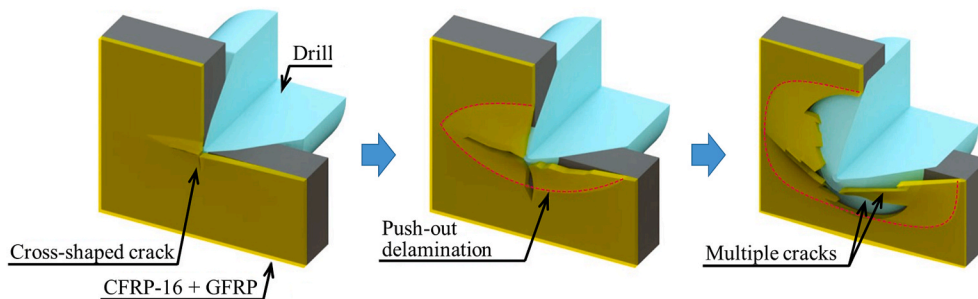


Fig. 7. Conceptual figure of the mechanism of damage propagation at drill-exit.

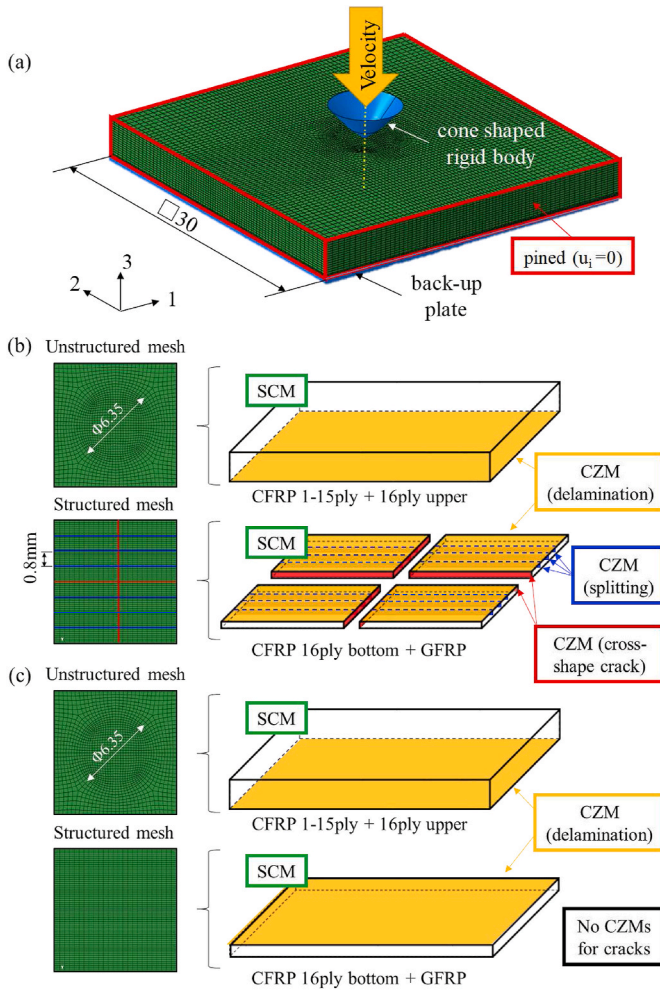


Fig. 8. (a) FEM model setup and boundary conditions for simplified drilling simulation, (b) Schematics of the multiple crack (MC) model, and (c) Schematics of the no crack (NC) model.

process after point C did not cause propagation of the delamination but removed the remaining region in the two outermost plies. This is because the thrust force applied only from outside the drill was not high enough to cause the delamination to progress.

Consequently, the bending behavior and the internal damages in additional GFRP ply significantly affect on the push-out delamination behavior. Therefore, the improvement of material properties (stiffness, strength, and fracture toughness) of additional ply has the great potential to suppress the extent of delamination.

The findings about the mechanisms of the push-out delamination obtained from the penetration and interruption tests are summarized below and illustrated in Fig. 7:

- The cross-shaped crack, consisting of the transverse crack in the CFRP 16-ply and the fiber breakages in the CFRP 16-ply and GFRP ply, formed immediately after the drill tip penetration (i.e. after the maximum thrust force).
- As drilling progressed, several transverse cracks formed in the CFRP 16-ply and divided the two unprocessed outermost plies into several strips.
- These transverse cracks and fiber breakages lowered the bending stiffness of the unprocessed region in the outermost plies. The out-of-plane bending of the unprocessed outermost plies caused the propagation of the push-out delamination.

- The extent of delamination may be controlled by adjusting the material properties of the additional ply. This is numerically examined in Section 3.2.

3. Numerical simulation

3.1. FEM model setup

This section develops a simplified simulation model using a meso-scale damage model to predict the push-out delamination during the drilling of composite laminates. The developed scheme is based on the simplified simulation model proposed by Duraõ et al. [2] and Park [9]. In the simplified simulation model, the drill is approximated by a circular cone, and only the feed rate is imposed on it. This means that the drilling is simplified into the quasi-static out-of-plane bending problem. The authors believe that this assumption is not too drastic for the prediction of the push-out delamination since the feed rate is the dominant factor and the spindle speed does not have a significant effect on it [4]. Fig. 8 (a) illustrates the simplified simulation model and boundary conditions. The simulation was conducted using Abaqus/Explicit [19]. In the simulation, only a 30 mm square region around the hole was modelled and all degrees of freedom on the nodes located on the sides of the specimen were fixed. The drill and the back-up plate were modelled as a rigid body. Contact between the drill and the laminate and between the back-up plate and the laminate was simulated using the general contact algorithm in Abaqus/Explicit [19]. In order to reduce the computational cost, the mass density of the laminate was scaled up 1000 times and the feed rate was scaled up 10 times while keeping the percentage of the kinetic energy under 2% of the strain energy.

As discussed in Section 2, the reduction in the bending stiffness of the unprocessed outermost plies due to the geometrical change caused by the drilling appears to be an important phenomenon. Thus, the element deletion method [9] was introduced to reproduce the actual contact condition between the drill and laminate. In this method, the elements in the processed region are removed when they are applied to the maximum force determined based on the sectional thrust force obtained from the experiment. The details of the calculation procedure of thrust distribution are described in Appendix A. In the complete model [16–18], the element deletion was done based on the strength and energy to consider the local energy balance when a new fracture plane is generated in one element. However, it is impossible to use these criteria in the simplified model where the actual fracture planes cut by the drill edge are not directly modelled. Alternatively, the simplified model considers the global energy balance between the total work done by the drill feed, stored strain energy in the laminates, and energy dissipated by the fracture at drill exit.

Additionally, the experiment-based mesoscale damage modelling approach [20], which combines continuous and discrete damage models based on experimental observations, was utilized to predict the various internal damages. Generally, the continuous damage model such as the smeared crack model (SCM) is computationally efficient and robust but it can easily underestimate the propagation of large cracks. In the composite laminates, the deterioration of the prediction accuracy of transverse cracks directly affects that of the delamination since the transverse crack and the delamination strongly interact with each other [21,22]. On the other hand, like the cohesive zone model (CZM), the discrete damage model is able to capture damage propagation including the interaction between the transverse cracks and delamination precisely, but is computationally expensive. Therefore, the experiment-based hybrid modelling strategy enables reasonably computationally-efficient modelling. As observed in the drilling experiments, relatively large cracks formed only in the two bottom plies, which consisted of several transverse cracks and fiber tensile failure in the outermost CFRP ply and fiber tensile failure in the additional ply. These cracks were accompanied by the push-out delamination. In order to model their interactions, we employed CZM for these cracks and the

Table 1
Material properties of T800S-3900-2B.

| | | T800S/3900-2B [25] | GFRP [29] |
|---|----------------|------------------------|------------------------|
| Density | ρ | 1800 kg/m ³ | 2500 kg/m ³ |
| Longitudinal Young's modulus | E_{11} | 153 GPa | 26 GPa |
| Transverse Young's modulus | E_{22} | 8 GPa | 26 GPa |
| Out-of-plane Young's modulus | E_{33} | 8 GPa | 8 GPa |
| In-plane shear modulus | G_{12} | 4.03 GPa | 3.8 GPa |
| Out-of-plane shear modulus | G_{23} | 2.75 GPa [26, 27] | 2.8 GPa |
| Out-of-plane shear modulus | G_{31} | 4.03 GPa | 2.8 GPa |
| In-plane Poisson's ratio | ν_{12} | 0.34 | 0.10 [30] |
| Out-of-plane Poisson's ratio | ν_{23} | 0.45 | 0.25 [30] |
| Out-of-plane Poisson's ratio | ν_{13} | 0.34 | 0.25 [30] |
| Longitudinal tensile strength | X^T | 3100 MPa | 850 MPa |
| Longitudinal compressive strength | X^C | 1242 MPa [27] | 720 MPa |
| Fracture toughness for fiber tensile failure | G_{1C}^T | 193.3N/mm | 50N/mm |
| Fracture toughness rate for fiber compressive failure | G_{1C}^C | 25.9N/mm | 50N/mm |
| Mode I maximum traction | t_1^0 | 66.9 MPa | 214 MPa |
| Mode II and III maximum traction | $t_{2,3}^0$ | 100 MPa | 38 MPa |
| Mode I fracture toughness | G_I^C | 0.2N/mm [28] | 3.47N/mm |
| Mode II and III fracture toughness | $G_{II,III}^C$ | 1.0N/mm [28] | 1.0N/mm ^a |

^a G_{II}^C and G_{III}^C in GFRP are estimated values.

push-out delamination. In contrast, no significant damage propagation was observed in the inner plies (Fig. 4). These damages were thus modelled by SCM. The peel up delamination is beyond the scope of the prediction. The schematic of the mesoscale damage model is shown in Fig. 8 (b). The laminate was divided into reduced integration solid elements (C3D8R). All plies other than the CFRP 16-ply were divided into one element in the thickness direction. The CFRP-16 ply where the push-out delamination was observed was divided into two elements in the thickness direction. To model the large multiple cracks in the two bottom plies and the push-out delamination, the surface-based CZM was introduced. While the CZM for splittings in the CFRP-16 ply were inserted parallel to the fiber direction, those for fiber failure in the CFRP-16 ply and woven GFRP ply were inserted perpendicular to the fiber direction. Additionally, the crack distance was set to 0.8 mm based on experimental observation. This value is consistent with the saturated crack density found in the tensile test of similar material reported in [23] and analytically predicted by Onodera et al. [24]. Therefore, when this model is applied to other materials and stackings, the crack distance can be determined based on experiment or analytical models. To examine the importance of modelling the transverse cracks for the prediction of push-out delamination, an additional simulation model with no cracks was prepared (Fig. 8 (c)). Hereafter, the simulation models with and without multiple cracks are named as MC and NC models, respectively. The details of SCM and CZM can be found in Refs. [19,20]. All material properties used in the simulation are summarized in Table 1 [25–30]. As discussed in Section 2.1, the push-out delamination happened inside the ply and not at the interface toughened by thermoplastic particles. In fact, the critical energy release rates at the toughened interface ($G_I^C = 0.54$ N/mm and $G_{II}^C = 1.54$ N/mm [25]) are relatively higher than those of general CFRP interface (e.g., $G_I^C = 0.2$ N/mm and $G_{II}^C = 1.00$ N/mm [28]). It was assumed that the critical energy release rates inside the ply in which there are no toughening particles are similar to those of the general CFRP interface since it is difficult to obtain them.

3.2. Results and discussion

In this section, first, several verifications of the proposed simplified

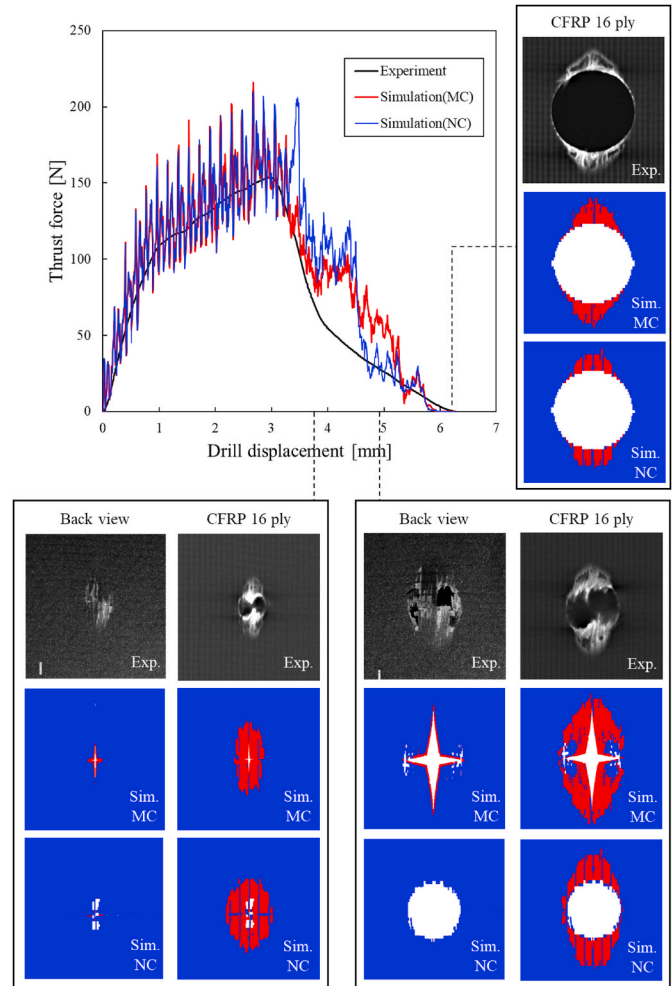


Fig. 9. Comparisons of the thrust history and damage propagation behavior with a feed rate of 375 mm/min between experiment and simulations using the MC and NC models.

model were carried out. Then, sensitivity studies were conducted to explore ways to mitigate the push-out delamination.

Firstly, the simulations using the MC and NC models were compared with the experiment under the condition of a spindle speed of 3200 rpm and a feed rate of 375 mm/min. Fig. 9 compares the thrust history and the damage growth between the experiment and simulations. As shown in Fig. 9, the length of the push-out delamination predicted by the NC model was shorter than that of the MC model. In the MC model, the delamination length at the center was the longest because the center transverse crack propagated easier than other cracks because of Mode I deformation and triggered the delamination. On the other hand, in the NC model, the delamination front became flat since no crack triggered the delamination. As a result, the delamination shape of the MC model is closer to the experimental result than the NC model. This result enhances the importance of modelling the transverse cracks in the prediction of push-out delamination. Additionally, Fig. 9 confirms that the predicted thrust history in the MC model is in good agreement with the experiment. One exception is the overestimation of thrust force at the displacement of 4.0–5.0 mm. As shown in the back view at a displacement of 5.0 mm, several regions of the outermost plies were removed in the experiment. However, this removal could not be reproduced in the simulation since these regions were cut by drill rotation, which was not actually reproduced in the simulation. Therefore, the simplified simulation overestimated the area of the unprocessed region and the resulting reaction force from it. This mismatch is the limitation of the

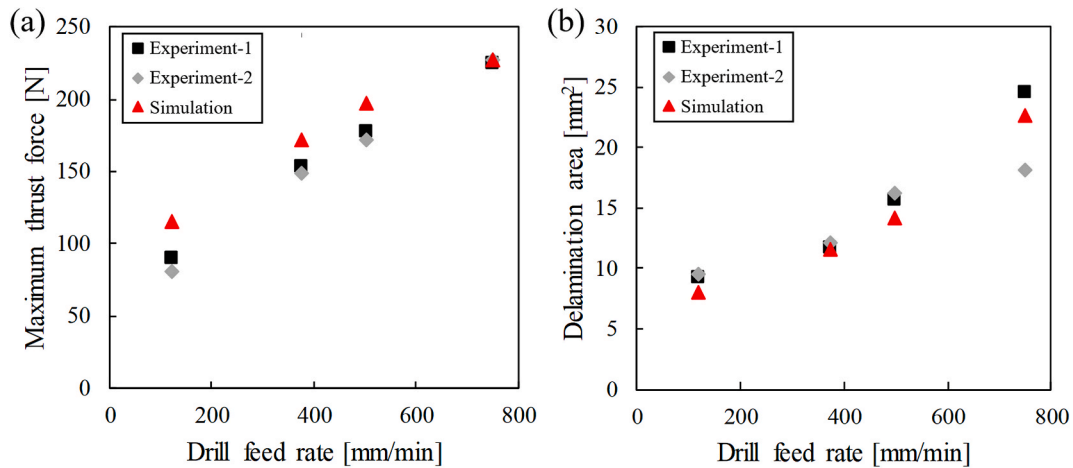


Fig. 10. Comparisons of predicted results by the MC model with experiments for each feed rate; (a) Maximum thrust force, (b) Delamination area.

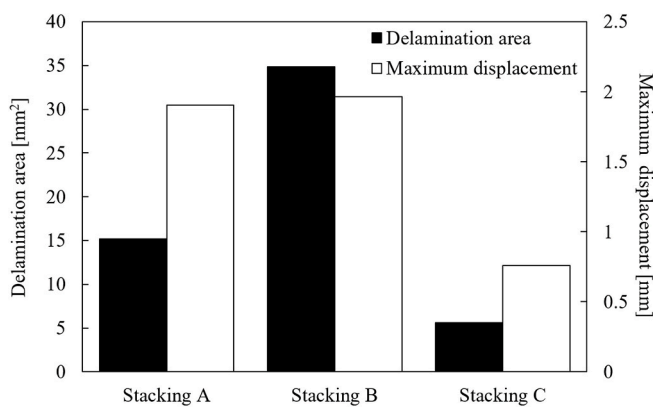


Fig. 11. Comparisons of the delamination area and maximum out-of-plane displacement with a feed rate of 375 mm/min between three different specimen configurations.

simplified simulation model. However, the simulation was able to reproduce the sequence of the internal damages (cross-shaped crack, several transverse cracks, and the push-out delamination) and the resultant residual delamination area. The authors thus believe that this mismatch is not a severe disadvantage from the perspective of engineering use of the simulation tool. In fact, the simplified simulation required only 3–5 h when using the 32 CPU workstation (Intel Xeon E5-2680 v3, 2.50 GHz). This CPU time is a few percent of that for the complete simulation model [16,18].

For more detailed verification of the MC model, simulations were conducted under the conditions of a spindle speed of 3200 rpm and feed rates of 120, 375, 500, and 750 mm/min. The comparisons of the predicted and experimental maximum thrust force and push-out delamination areas are summarized in Fig. 10(a) and (b). Here, the predicted maximum thrust force is obtained from the moving average of 20 points of raw data from the simulation because numerical oscillation is inevitable in the drilling simulation where discontinuous contact happens. In all feed rates, the proposed model can accurately predict the maximum thrust force and the delamination area. From these results, it was concluded that the proposed simplified simulation with the experiment-based mesoscale damage model is useful for the computationally efficient prediction of the thrust history, damage scenario, maximum thrust force, and residual delamination area.

Finally, the drilling simulations with different specimen configurations were performed to explore the way to reduce push-out delamination. In addition to the original specimen configuration, two specimen

configurations were prepared as follows.

- Stacking A CFRP[0/ - 45/90/45]_{2S} + GFRP[0, 90] (original)
- Stacking B CFRP[0₂/ - 45₂/90₂/45₂]_{2S} + GFRP[0, 90]
- Stacking C CFRP[0/ - 45/90/45]_{2S} + CFRP[0, 90]

By comparing Stacking A with B, it is possible to understand the effect of ply thickness on the drilling damage. This is one of the size effect well-known in the polymers and polymer composites [28,31–35]. On the other hand, the comparison between Stackings A and C will provide us the knowledge needed to control the drilling damage by adjusting the material properties of the additional ply on the bottom side. In the woven CFRP ply of Stacking C, the longitudinal elastic and fracture properties of T800S/3900-2B were assumed in both in-plane directions. The predicted delamination areas and maximum out-of-plane displacements are compared in Fig. 11. Here, the maximum out-of-plane displacement is obtained at the center nodes of additional ply before their elements were removed by the drilling. It can be seen from Fig. 11 that there is a clear size effect of ply thickness in the drilling damage. The thicker ply laminate (Stacking B) resulted in a larger delamination area than the thinner ply laminate (Stacking A). This is because the transverse cracks that trigger the push-out delamination have an in-situ effect [36,37]. As discussed in the references [36,37], the transverse cracks propagate easier in the thick ply than in the thin ply. Consequently, applying a thinner CFRP ply at the bottom side is useful in reducing the drilling damage. Furthermore, by comparing Stackings A and C, it was confirmed that the stiffer and stronger additional ply successfully reduced the out-of-plane deflection and resultant delamination area. These results show that delamination can be controlled by adjusting the material properties of the additional ply on the bottom side.

4. Conclusions

This study conducted an experimental and numerical investigation into the push-out delamination during the drilling of composite laminates. In the experiment, the penetration and interruption tests were carried out to determine the damage progression mechanism during the drilling process. From these experiments, the following damage scenario was revealed; (i) after the drill tip penetration, several damages in the outermost plies (transverse cracks in CFRP and fiber breakage in CFRP and GFRP) reduce the bending stiffness, (ii) bending (not drilling) results in propagation of delamination. From these findings, the experiment-based mesoscale damage model was developed. Transverse cracks and fiber breakage in the bottom two plies, which are considered

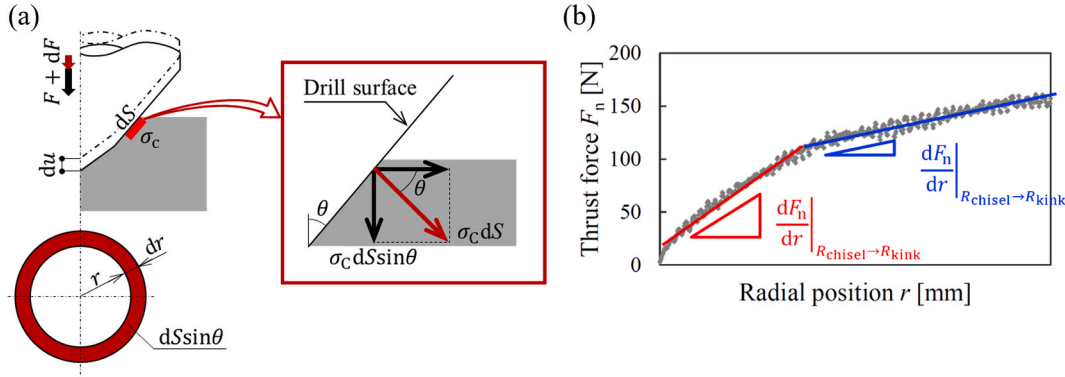


Fig. A1. Definition of sectional thrust force.

to be the dominant events against the push-out delamination, were modelled by CZM. The fiber breakages in the other regions, which did not propagate largely, were modelled by SCM. These damage models were implemented in the simplified drilling simulation model, in which the drilling was approximated as an out-of-plane bending problem by the conical. The developed simulation scheme was able to predict the thrust history and delamination propagation in all feed rates. It was thus confirmed that the developed tool is a useful engineering tool to determine the drilling conditions for low residual damage. Furthermore, based on the sensitivity studies conducted using the proposed model, it was concluded that the extent of delamination can be controlled by adjusting the thickness and material properties of the bottom plies.

CRedit authorship contribution statement

R. Higuchi: Conceptualization, Methodology, Software, Writing - original draft, Writing - review & editing. **S. Warabi:** Software, Validation, Investigation. **W. Ishibashi:** Software, Validation, Investigation.

T. Okabe: Supervision, Conceptualization.

Declaration of competing interest

The authors declare that they have no known competing financial interests or personal relationships that could have appeared to influence the work reported in this paper.

Acknowledgements

This study was partially supported by the New Energy and Industrial Technology Development Organization (NEDO) (Project No. P08024, No. P15006). This study was also supported by the Council for Science, Technology and Innovation (CSTI), the Cross-ministerial Strategic Innovation Promotion Program (SIP), and the 'Materials Integration' for revolutionary design system of structural materials (Funding agency: Japan Science and Technology Agency (JST)).

Appendix A. Calculation procedure of thrust distribution

In this study, the drilling is simplified to an out-of-plane bending problem caused by the feeding of a conical, whose shape is the same as the rotating shape of the drill. In the simulation, the drilling process is modelled using the element deletion method. In this method, the elements are removed when they are subjected to maximum stress $\sigma_c(r)$. By considering the increment of thrust force dF during the infinitesimal feed of drill, as shown in Fig. A1 (a), the maximum stress can be determined as follows.

$$dF = \sigma_c(r)dS\sin\theta = \sigma_c(r)2\pi r dr \Leftrightarrow \sigma_c(r) = \frac{1}{2\pi r} \frac{dF}{dr}, \tag{A.1}$$

where, dF/dr can be calculated from the relationship between the thrust force and radial position as shown in Fig. A1 (b). Here, the radial position is calculated using the drill tip position and drill geometry. From Fig. A1 (b), dF/dr is discontinuous at R_{kink} where the point angle changes from 108° to 90° . Additionally, we assumed that the specimen at the chisel edge region is subjected to pure transverse compression. Consequently, the distribution of maximum stress $\sigma_c(r)$ results in

$$\sigma_c(r) = \begin{cases} Y_c & (r \leq R_{chisel}) \\ k_{area} \cdot \frac{1}{2\pi r} \frac{dF}{dr} \Big|_{r \leq R_{kink}} & (R_{chisel} \leq r \leq R_{kink}) \\ k_{area} \cdot \frac{1}{2\pi r} \frac{dF}{dr} \Big|_{R_{kink} \leq r} & (R_{kink} \leq r) \end{cases}, \tag{A.2}$$

where, Y_c is the transverse compressive strength, R_{chisel} is the chisel edge radius, and k_{area} is the correction factor of the contact area. In the drilling simulation, remeshing is necessary to ensure the processed surface is along the drill surface, however, this results in high computational cost. Therefore, in this study, the laminate is divided by the general structural mesh. In this case, the drilled surface of the specimen becomes step-wise and the contact area is underestimated. In order to correct the contact area in the simulation with the structural mesh to the ideal contact area between the conical and laminate, a correction factor k_{area} was introduced. k_{area} was determined based on the simulation with a certain feed rate; the same factor is used for the other feed rate as it only depends on the FEM mesh and the drill shape. The determined values are as follows.

$$k_{\text{area}} = \begin{cases} 9.0 & (R_{\text{chisel}} \leq r \leq R_{\text{kink}}) \\ 3.0 & (R_{\text{kink}} \leq r) \end{cases}. \quad (\text{A.3})$$

References

- [1] V.N. Gaitonde, S.R. Karnik, J.C. Rubio, A.E. Correia, A.M. Abrão, J.P. Davim, A study aimed at minimizing delamination during drilling of CFRP composites, *J. Compos. Mater.* 45 (22) (2011) 2359–2368, <https://doi.org/10.1177/0021998311401087>.
- [2] L.M.P. Durão, M.F.S.F. de Moura, A.T. Marques, Numerical prediction of delamination onset in carbon/epoxy composites drilling, *Eng. Fract. Mech.* 75 (9) (2008) 2767–2778, <https://doi.org/10.1016/j.engfracmech.2007.03.009>.
- [3] A.T. Marques, L.M.P. Durão, A.G. Magalhães, J.F. Silva, J.M.R.S. Tavares, Delamination analysis of carbon fibre reinforced laminates: evaluation of a special step drill, *Compos. Sci. Technol.* 69 (14) (2009) 2376–2382, <https://doi.org/10.1016/j.compscitech.2009.01.025>.
- [4] D. Liu, Y. Tang, W.L. Cong, A review of mechanical drilling for composite laminates, *Compos. Struct.* 94 (4) (2012) 1265–1279, <https://doi.org/10.1016/j.compstruct.2011.11.024>.
- [5] I. Shyha, S.L. Soo, D. Aspinwall, S. Bradley, Effect of laminate configuration and feed rate on cutting performance when drilling holes in carbon fibre reinforced plastic composites, *J. Mater. Process. Technol.* 210 (8) (2010) 1023–1034, <https://doi.org/10.1016/j.jmatprotec.2010.02.011>.
- [6] U.A. Khashaba, Delamination in drilling GFR-thermoset composites, *Compos. Struct.* 63 (3–4) (2004) 313–327, [https://doi.org/10.1016/s0263-8223\(03\)00180-6](https://doi.org/10.1016/s0263-8223(03)00180-6).
- [7] U.A. Khashaba, I.A. El-Sonbaty, A.I. Selmy, A.A. Megahed, Machinability analysis in drilling woven GFR/epoxy composites: Part I – effect of machining parameters, *Compos. Part A-Appl. S.* 41 (3) (2010) 391–400, <https://doi.org/10.1016/j.compositesa.2009.11.006>.
- [8] U.A. Khashaba, I.A. El-Sonbaty, A.I. Selmy, A.A. Megahed, Machinability analysis in drilling woven GFR/epoxy composites: Part II – effect of drill wear, *Compos. Part A-Appl. S.* 41 (9) (2010) 1130–1137, <https://doi.org/10.1016/j.compositesa.2010.04.011>.
- [9] S. Park, report Characteristics of Drilling Process on Composite Laminates: Understanding Damage Initiation and Progression to Improve Final Hole Quality, (PhD thesis).
- [10] E. Kilickap, Optimization of cutting parameters on delamination based on taguchi method during drilling of GFRP composite, *Expert Syst. Appl.* 37 (8) (2010) 6116–6122, <https://doi.org/10.1016/j.eswa.2010.02.023>.
- [11] V.N. Gaitonde, S.R. Karnik, J.C. Rubio, A.E. Correia, A.M. Abrão, J.P. Davim, Analysis of parametric influence on delamination in high-speed drilling of carbon fiber reinforced plastic composites, *J. Mater. Process. Technol.* 203 (1–3) (2008) 431–438, <https://doi.org/10.1016/j.jmatprotec.2007.10.050>.
- [12] S.R. Karnik, V.N. Gaitonde, J.C. Rubio, A.E. Correia, A.M. Abrão, J.P. Davim, Delamination analysis in high speed drilling of carbon fiber reinforced plastics (CFRP) using artificial neural network model, *Mater. Des.* 29 (9) (2008) 1768–1776, <https://doi.org/10.1016/j.matdes.2008.03.014>.
- [13] C.C. Tsao, Taguchi analysis of delamination associated with various drill bits in drilling of composite material, *Int. J. Mach. Tool Manufact.* 44 (10) (2004) 1085–1090, [https://doi.org/10.1016/s0890-6955\(04\)00054-9](https://doi.org/10.1016/s0890-6955(04)00054-9).
- [14] A. Faraz, D. Biermann, K. Weinert, Cutting edge rounding: an innovative tool wear criterion in drilling CFRP composite laminates, *Int. J. Mach. Tool Manufact.* 49 (15) (2009) 1185–1196, <https://doi.org/10.1016/j.ijmactools.2009.08.002>.
- [15] R. Zitoun, F. Collombet, Numerical prediction of the thrust force responsible of delamination during the drilling of the long-fibre composite structures, *Compos. Part A-Appl. S.* 38 (3) (2007) 858–866, <https://doi.org/10.1016/j.compositesa.2006.07.009>.
- [16] V.A. Phadnis, F. Makhadmeh, A. Roy, V.V. Silberschmidt, Drilling in carbon/epoxy composites: experimental investigations and finite element implementation, *Compos. Part A-Appl. S.* 47 (2013) 41–51, <https://doi.org/10.1016/j.compositesa.2012.11.020>.
- [17] O. Isbilir, E. Ghassemieh, Numerical investigation of the effects of drill geometry on drilling induced delamination of carbon fiber reinforced composites, *Compos. Struct.* 105 (2013) 126–133, <https://doi.org/10.1016/j.compstruct.2013.04.026>.
- [18] N. Feito, J. López-Puente, C. Santiuste, M. Miguélez, Numerical prediction of delamination in CFRP drilling, *Compos. Struct.* 108 (2014) 677–683, <https://doi.org/10.1016/j.compstruct.2013.10.014>.
- [19] Abaqus, 6.13 Documentation, Dassault Systemes Simulia Corporation.
- [20] R. Higuchi, T. Okabe, A. Yoshimura, T.E. Tay, Progressive failure under high-velocity impact on composite laminates: experiment and phenomenological mesomodelling, *Eng. Fract. Mech.* 178 (2017) 346–361, <https://doi.org/10.1016/j.engfracmech.2017.03.019>.
- [21] B.Y. Chen, T.E. Tay, S.T. Pinho, V.B.C. Tan, Modelling delamination migration in angle-ply laminates, *Compos. Sci. Technol.* 142 (2017) 145–155, <https://doi.org/10.1016/j.compscitech.2017.02.010>.
- [22] A. Ramji, Y. Xu, M. Yasae, M. Grasso, P. Webb, Delamination migration in CFRP laminates under mode I loading, *Compos. Sci. Technol.* 190 (2020), <https://doi.org/10.1016/j.compscitech.2020.108067>, 108067.
- [23] S. Ogihara, S. Kobayashi, N. Takeda, A. Kobayashi, Damage mechanics characterization of transverse cracking behavior in high-temperature CFRP laminates, *Compos. Sci. Technol.* 61 (8) (2001) 1049–1055, [https://doi.org/10.1016/s0266-3538\(00\)00236-0](https://doi.org/10.1016/s0266-3538(00)00236-0).
- [24] S. Onodera, Y. Nagumo, T. Okabe, Prediction for progression of transverse cracking in CFRP cross-ply laminates using Monte Carlo method, *Adv. Compos. Mater.* 26 (5) (2017) 477–491, <https://doi.org/10.1080/09243046.2017.1325076>.
- [25] T. Morimoto, S. Sugimoto, H. Katoh, E. Hara, T. Yasuoka, Y. Iwahori, T. Ogasawara, S. Ito, Jaxa advanced composites database, jaxa research and development memorandum, 2015. Tech. rep., JAXA-RM-14-004, ISSN 1349-1121 (in Japanese), <https://repository.exst.jaxa.jp/dspace/handle/a-is/185731>.
- [26] K. Shigemori, Fatigue strength properties of interlaminar toughened CFRP laminates under cyclic loading in the out-of-plane direction, *Trans. JSME* 80 (812) (2014). SMM0087 (in Japanese).
- [27] T. Yokozeki, T. Ogasawara, T. Ishikawa, Nonlinear behavior and compressive strength of unidirectional and multidirectional carbon fiber composite laminates, *Compos. Part A-Appl. S.* 37 (11) (2006) 2069–2079, <https://doi.org/10.1016/j.compositesa.2005.12.004>.
- [28] S.R. Hallett, B.G. Green, W.G. Jiang, M.R. Wisnom, An experimental and numerical investigation into the damage mechanisms in notched composites, *Compos. Part A-Appl. S.* 40 (5) (2009) 613–624, <https://doi.org/10.1016/j.compositesa.2009.02.021>. URL.
- [29] R. Hosseinzadeh, M.M. Shokrieh, L. Lessard, Damage behavior of fiber reinforced composite plates subjected to drop weight impacts, *Compos. Sci. Technol.* 66 (1) (2006) 61–68, <https://doi.org/10.1016/j.compscitech.2005.05.025>.
- [30] C. Menna, D. Asprone, G. Caprino, V. Lopresto, A. Prota, Numerical simulation of impact tests on GFRP composite laminates, *Int. J. Impact Eng.* 38 (8–9) (2011) 677–685, <https://doi.org/10.1016/j.ijimpeng.2011.03.003>.
- [31] Z.P. Bazant, I.M. Daniel, Z. Li, Size effect and fracture characteristics of composite laminates, *J. Eng. Mater-T ASME* 118 (3) (1996) 317–324, <https://doi.org/10.1115/1.2806812>.
- [32] M. Salviato, K. Kirane, S.E. Ashari, Z.P. Bazant, G. Cusatis, Experimental and numerical investigation of intra-laminar energy dissipation and size effect in two-dimensional textile composites, *Compos. Sci. Technol.* 135 (2016) 67–75, <https://doi.org/10.1016/j.compscitech.2016.08.021>.
- [33] M. Salviato, K. Kirane, Z.P. Bazant, G. Cusatis, Mode I and II interlaminar fracture in laminated composites: a size effect study, *J. Appl. Mech.* 86 (9) (2019), 091008, <https://doi.org/10.1115/1.4043889>.
- [34] Y. Qiao, M. Salviato, Strength and cohesive behavior of thermoset polymers at the microscale: a size-effect study, *Eng. Fract. Mech.* 213 (2019) 100–117, <https://doi.org/10.1016/j.engfracmech.2019.03.033>.
- [35] R. Higuchi, T. Okabe, T. Nagashima, Numerical simulation of progressive damage and failure in composite laminates using XFEM/CZM coupled approach, *Compos. Part A-Appl. S.* 95 (2017) 197–207, <https://doi.org/10.1016/j.compositesa.2016.12.026>.
- [36] G.J. Dvorak, N. Laws, Analysis of progressive matrix cracking in composite laminates II. first ply failure, *J. Compos. Mater.* 21 (4) (1987) 309–329, <https://doi.org/10.1177/002199838702100402>.
- [37] S. Onodera, T. Okabe, Three-dimensional analytical model for effective elastic constants of transversely isotropic plates with multiple cracks: application to stiffness reduction and steady-state cracking of composite laminates, *Eng. Fract. Mech.* 219 (2019), <https://doi.org/10.1016/j.engfracmech.2019.106595>, 106595.